THEORETICAL DETECTION OF A DARK CONTRAST LINE IN TWINNED APATITE BICRYSTALS AND ITS POSSIBLE CORRELATION WITH THE CHEMICAL PROPERTIES OF HUMAN DENTIN AND ENAMEL CRYSTALS

E. F. BRÈS,* W. G. WADDINGTON,‡ J.-C. VOEGEL,* J. C. BARRY,‡‖ AND R. M. FRANK*
Unité de Recherches INSERM U157, UFR d'Odontologie, Université Louis Pasteur, 67000 Strasbourg, France; ‡Department of Metallurgy and Science of Materials, University of Oxford, Oxford OX1 3PH, Great Britain; and ‖Center for Solid State Science, Arizona State University, Tempe, Arizona 85287

ABSTRACT Electron microscope images of twinned apatite bicrystals oriented along the $[11\bar{2}0]$ crystallographic direction have been simulated for various experimental conditions, and the validity of the calculation has been checked. These images show a dark contrast line similar to the one observed experimentally in enamel and dentin crystals and therefore strongly suggest the presence of a twin plane parallel to the $(1\bar{1}00)$ crystallographic planes, in these crystals. The presence of a twin boundary in teeth and bone crystals is of prime importance for the adsorption and the dissolution properties of the calcified tissues as a whole.

INTRODUCTION

Human enamel (Fig. 1), dentin, and bone tissues are composed of a mineral phase which can be approximated by a multitude of poorly crystalline carbonated hydroxyapatite microcrystals embedded in an organic matrix. In the case of human enamel, these crystals have a flat hexagonal shape. Their approximate dimensions are: 50-nm thick, 90-nm wide, and can be several micrometers long (Fig. 2). During the carious dissolution process, enamel apatite crystals are first attacked on their basal planes leading to the formation of an hexagonal lesion elongated along the $[11\bar{2}0]$ direction and running through the crystals parallel to the $[0001]$ direction. This lesion is limited by the $(10\bar{1}0)$, $(01\bar{1}0)$, and $(1\bar{1}00)$ lattice planes while it develops through the crystals at a rate five times faster along the c axis than along the a_1, a_2, and a_3 axes (Voegel and Frank, 1977; Jongebloed et al., 1974). On the basis of surface energy calculations (Arends, 1973; Arends and Jongebloed, 1977), the anisotropy of the dissolution has been interpreted as being due to a strain field generated in the crystals by a screw dislocation of Burgers vector parallel in the $[0001]$ direction. These works are in agreement with the investigations made by Lovell (1958). Patel et al. (1966), and Phakey and Leonard (1970), who have shown by acid etching and x-ray topography that dislocations of the screw type with Burgers vector $\mathbf{b} = c[0001]$ are often present in the hydroxyapatite lattice. However, these observations do not explain the elongated shape of the lesion, as it would be expected from a single dislocation (Gilman et al., 1958); no explanation was given, either, for the presence of several initial dissolution sites aligned along $[11\bar{2}0]$ as can sometimes be observed. Brès et al. (1984) have identified three types of disorder that may act as dissolution sites: (*a*) regions of lattice buckling with departure from hexagonal symmetry, (*b*) dislocations, and (*c*) grain and twin boundaries. They have also suggested that the low angle grain boundary they have observed in crystals oriented along $[11\bar{2}0]$ could be twisted around $[1\bar{1}00]$ and give rise to a series of screw dislocations of Burgers vector parallel to $[0001]$ and situated on the boundary. These dislocations could correspond to the very initial dissolution sites of hexagonal shape observed in enamel crystals oriented along the $[0001]$ direction.

The observations concerning the location and the crystallographic structure of the initial dissolution sites of human enamel crystals can be correlated to observations made by several authors (Rönnholm, 1962; Nylen et al., 1963; Frazier, 1968; Voegel, 1978; Marshall and Lawless, 1981; Nakahara, 1982; Nakahara and Kakei, 1983, 1984) about the presence of a dark contrast line (DCL) parallel to the $[1\bar{1}00]$ lattice plane and situated at the same place as the initial dissolution sites (i.e., the center) of human enamel and dentine crystals oriented along the $[0001]$ or the $[11\bar{2}0]$ directions when observed with an electron microscope. The DCL is characterized by a contrast line up to 2.5-nm thick (Rönnholm, 1962) which disappears at Gaussian focus and changes contrast at de- and over-focus. The frequency of observation of the DCL is variable since Rönnholm (1962) has observed it in only 20% of the crystals, whereas Marshall and Lawless (1981) have

FIGURE 1 Electron micrograph of a human enamel crystal showing a dark line.

observed it in all crystals. It is important to note that the DCL is being observed independently of the experimental conditions used, since it has been observed in specimen prepared by diamond knife ultramicrotomy (Rönnholm, 1962; Voegel, 1978; Nakahara, 1982; Nakahara and Kakei, 1983, 1984), manual grinding (Nylen et al., 1963; Frazier, 1968), and ion milling (Marhsall and Lawless, 1981), under various imaging conditions: accelerating voltages of 80, 100, and 200 kV and with electron microscope objective lenses showing different spherical aberration coefficients. So, it can reasonably be thought that the DCL is not an artifact due to the specimen preparation or the electron imaging process. On the basis of the observations made so far, several hypotheses concerning the DCL have been put forward. These hypotheses can all be reduced to two: (*a*) the DCL is due to a structural variation inside the crystals, and (*b*) the DCL is due to atomic substitutions inside the crystal and at the line. Since both the DCL and the initial crystal dissolution phenomena occur at the same place inside human enamel and dentin crystals, it can reasonably be thought that they are correlated, so any advance towards the understanding of the DCL will bring better understanding of the pathological dissolution process of human apatite crystals during diseases such as

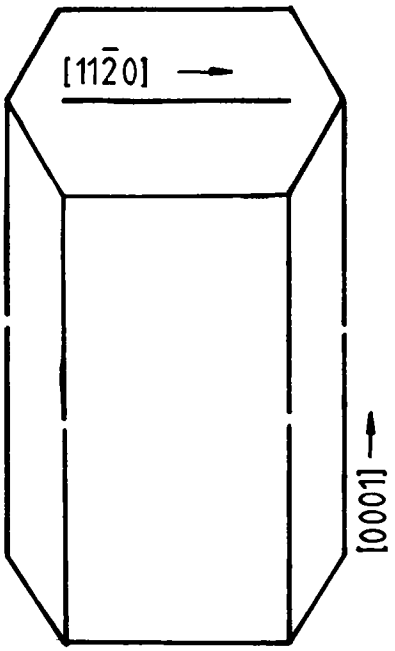

FIGURE 2 Schematic diagram of a human enamel apatite crystal showing the [$11\bar{2}0$] and the [0001] crystallographic directions.

dental caries or bone resorption and in the long term permit the development of inhibiting mechanisms to biological apatite crystal dissolution.

In the present study, we have carried out computer image simulations of twinned crystals of various thickness and at various defocus values. The validity of the calculation has been checked at a high resolution by comparing the image contrast away from the defect in a twinned and an untwinned hydroxyapatite structure. The microscope parameters used correspond to a microscope with which the DCL has been imaged by several authors (i.e., the 100B electron microscope [JEOL USA, Peabody, MA]).

MATERIALS AND METHODS

Structure of the Bicrystals

Four types of structures of bicrystals have been considered in this study: (*a*) twinned hydroxyapatite (TH), (*b*) twinned monoclinic hydroxyapatite (TMH), (*c*) twinned fluorapatite (TF), and (*d*) calcium-depleted twinned hydroxyapatite (CDTH). In all of these crystals a reflection twin parallel to [$11\bar{2}0$] was constructed as suggested by Rachinger et al. (1982) and on the basis of the atomic positions determined by Kay et al. (1964) (Fig. 3). No local strain due to twinning dislocation was assumed. The atomic positions have been adjusted to fulfil a perfect mirror symmetry with respect to the twin plane and to conserve the overall chemical charge balance in each bicrystal. However, a twin boundary requires an inverted operation and thus an additional defect for closure of the periodically continued unit. This was taken into account by the construction of a "super cell" composed of six hydroxyapatite unit cells separated by a defect plane every three cells (Fig. 4). The parameters for this "super cell" are: (*a*) 49.01 Å, (*b*) 9.43 Å, and (*c*) 6.88 Å. The distance between each defect is 24.50 Å. At the defect plane, the major change concerned the position of the PO_4^{3-} groups usually situated near the edge of the untwinned hydroxyapatite unit cell which were shifted so that the P as well as 2 O atoms lay on the twin plane and the two other O atoms lay

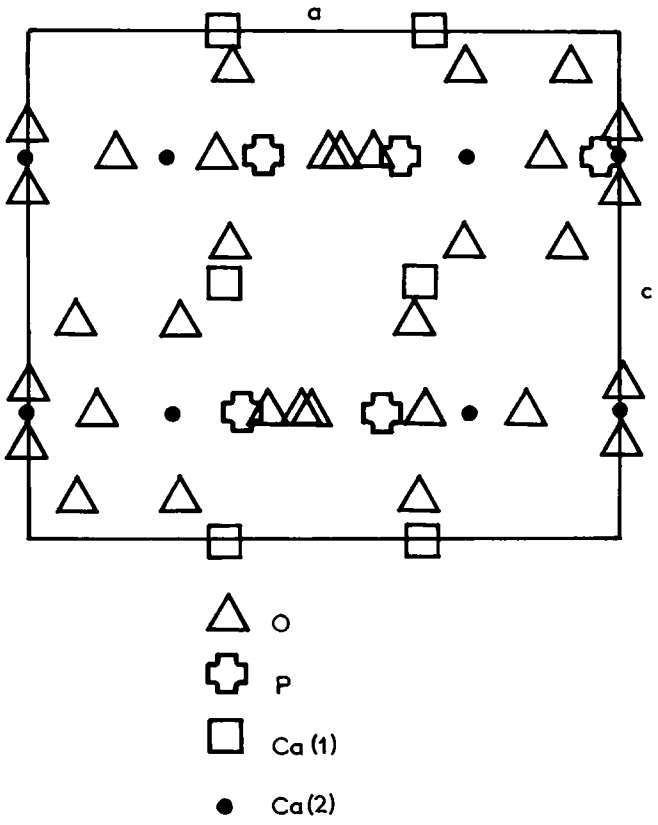

FIGURE 3 Schematic diagram of an hydroxyapatite unit cell viewed along the [$11\bar{2}0$] direction.

on each side of it (Figs. 3 and 4). The differences between the four cases studied are the following: in case I (TH), apart from the changes described above, the initial hydroxyapatite structure was used; the random positions of the hydroxyl groups above and below the Ca(2) planes were taken into account by setting the occupancy factor to 0.5 for these ions. In case II (TMH), a monoclinc hydroxyapatite structure was constructed by setting opposite positions of the hydroxyl groups above and below the Ca(2) planes in each bicrystal. In case III (TF), the fluorapatite structure was used. This implies that the F^- ions in the unit cell must be situated inside the Ca(2) triangles. In case IV (CDTH), an incipient dissolution of the bicrystals was simulated by setting the occupancy factor of the Ca atoms on the twin plane to zero.

Image Calculation Procedure

The basis of the image calculation computer program used in this study lies in the *n*-beam diffraction theory developed by Cowley and Moodie (1957) which describes the transmission of electrons through a sample by the transmission through a set of *N* two-dimensional phase and amplitude

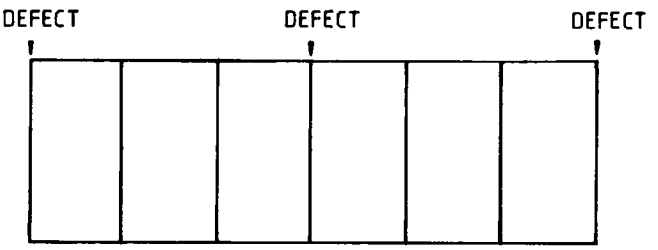

FIGURE 4 Diagram of the "super-cell" used for the calculation.

objects separated by a distance Δz. The total phase change and amplitude change of the electron wave in a slice of a specimen of thickness Δz is considered to take place in one plane. Then the propagation of the wave from one such a plane to the next is by Fresnel diffraction in which the thickness of the slice Δz goes to zero and the number of the slices N goes to infinity in such a way that $N\Delta z = T$, where T is the specimen thickness. This form of description becomes a rigorous representation of the scattering process completely consistent with the more conventional quantum mechanical descriptions. With the program used, the images are obtained in two steps: (*a*) calculation of the diffraction amplitudes, and (*b*) calculation of the image contrast by Fourier transformation of the diffraction amplitudes obtained. Much care is required for the calculation of images of crystals with periodically repeated planar defects. As we have already said, a twin boundary requires an additional defect for closure of the "super cell" used in the calculation. If the distance between adjacent defect is too small, diffuse scattering from the different defects interferes and leads to a reciprocal space distribution which is very different from that of a single defect (Wood et al., 1984). Accurate deconvolution of the diffuse scattering in image formation requires many reciprocal-space sampling points. This can place extreme demands on the size of the computations or severely limit the accuracy of the simulations. For this paper, we have developed a computer image simulation program permitting the sampling of 256 × 256 points in the super cell (52 points/nm of specimen are sampled) (Waddington, W. G., personal communication). The validity of the calculation of the images was checked at high resolution by comparing the contrast from the twinned structure to the one arising from an untwinned one.

The specimen characteristics and the microscope operating parameters are included in the calculation as follows: the specimen is described by its types of atoms, positions, and temperature factors, as well the projection direction, the number of beams, and the individual slice thickness. The operating microscope parameters are included in the calculation as follows: (*a*) the accelerating voltage of the microscope is used for the calculation of the energy of the electrons incident on the specimen; (*b*) the radius and position of the objective aperture are taken into account by the multiplication of the propagation function by an adequate aperture function; (*c*) the defect of focus and the spherical and chromatic aberration constants of the microscope objective lens are simulated by a selective phase delay of the beams generated by the specimen; and (*d*) the divergence of the beam incident on the specimen in the electron microscope is included in the calculation of in-focus images by calculating the variation of intensities of the diffracted beams with angle of incidence up to a known divergence, and summed in the image up to this angle (O'Keefe and Buseck, 1979; O'Keefe, 1973; Lynch et al., 1975).

Parameters Used in the Calculation

The structure of the super cell used in the calculation is shown in Figs. 4 and 5. It is composed of two bicrystals; each of these bicrystals is composed of three hydroxyapatite unit cells modified in such a way as to present a defect plane at each side of the bicrystal. The unit cell parameters of the super cell are the following: (*a*) 49.011 Å, (*b*) 9.432 Å, and (*c*) 6.881 Å. The separation between adjacent defects was 24.506 Å. The 100B microscope (JEOL USA) parameters used for the calculation of the images were: accelerating voltage, 100 kV; spherical aberration coefficient, 1.8 mm; beam divergence, 1 mrad; half width of Gaussian spread of focus (Δ value), 100 Å; a value of objective aperture of 0.278 $Å^{-1}$ corresponding to the optimum resolution of the microscope ($\simeq$ 3.6 Å) was chosen. The microscope parameters used to check the validity of the image calculation at high resolution correspond to the parameters of the ISI EM-002A microscope, which is to our knowledge the 100 kV accelerating voltage microscope showing the highest resolution. These parameters were: spherical aberration coefficient, 0.3 mm; beam divergence, 1 mrd; Δ value, 30 Å. The objective aperture used was 0.435 $Å^{-1}$; it

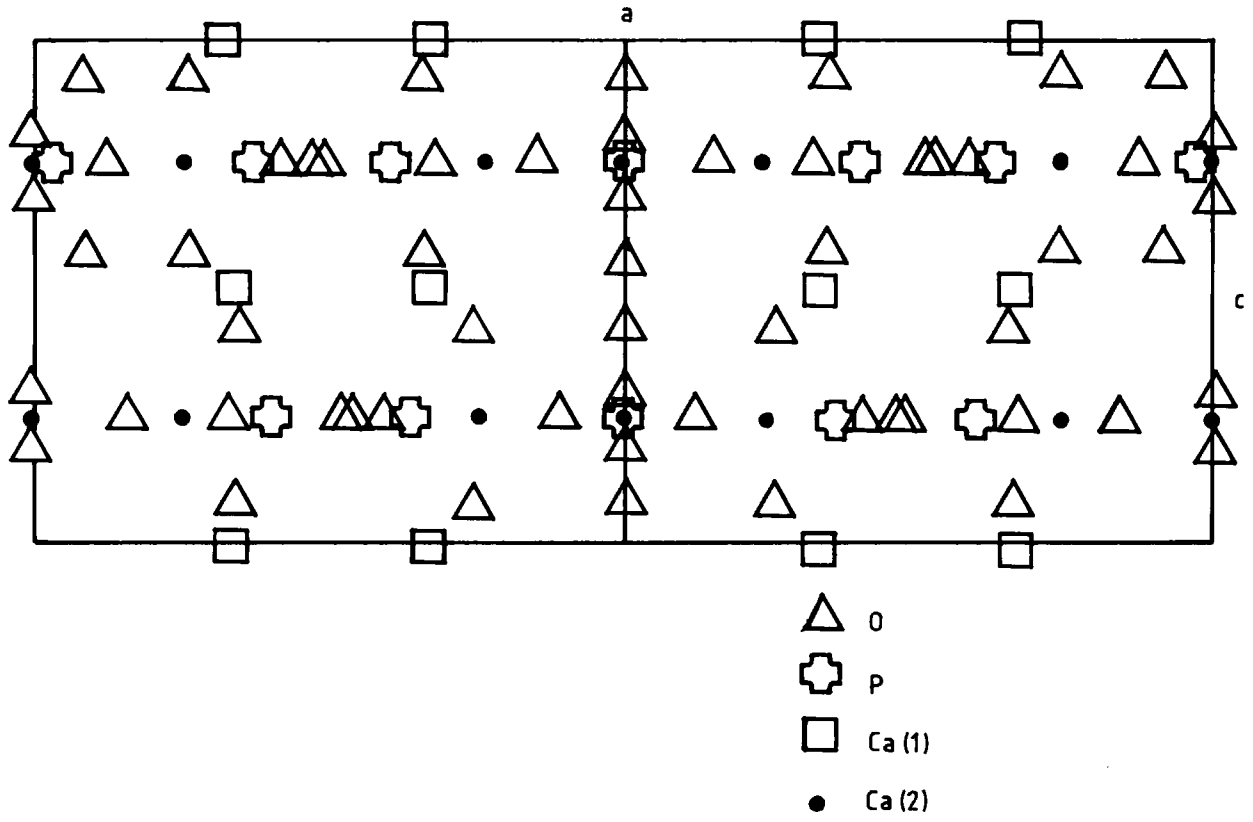

FIGURE 5 Schematic diagram of the atomic positions near a defect plane when viewed along the [$11\bar{2}0$] direction.

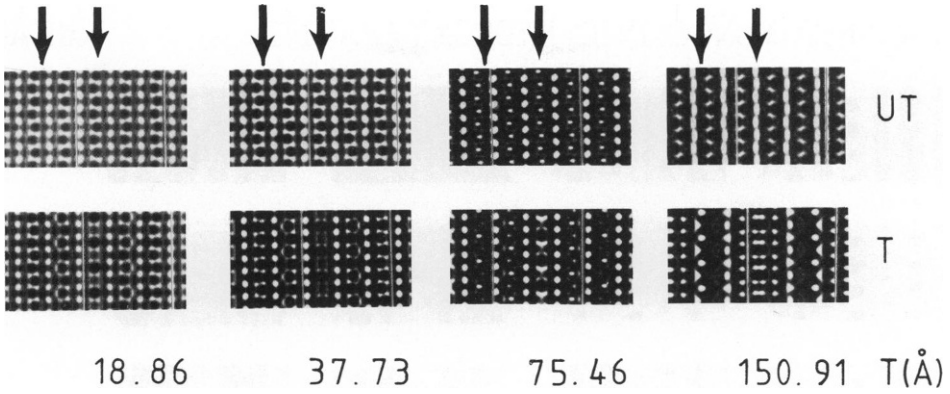

FIGURE 6 Images calculated at high resolution for an untwinned (UT) and a twinned (T) hydroxyapatite structures.

corresponds to a resolution of 2.3 Å. For these calculations the optimum focus was used (≃ −400 Å).

A slice thickness and a number of beams of respectively 2.358 Å and 1,771 were chosen to obtain a correlation test of 0.99995. The slice thickness values were the following: T1, 18.864 Å (8 slices); T2, 37.728 Å (16 slices); T3, 75.456 Å (32 slices); T4, 150.92 Å (64 slices). The following (de)focus values were used: −1,000 Å (Scherzer focus). −500 Å, 0 (Gaussian focus), 500 Å, and 1,000 Å. A negative value of the (de)focus value corresponds to a decrease of the lens current with respect to the one selected for Gaussian focus.

RESULTS

The images calculated for one super cell of each structure are characterized by a matrix of points on a microfiche printer to minimize contrast differences between different images. The maximum and minimum intensity values as well as the image contrast is identical for all images. Prints of the images on the microfiches have been included in Figs. 7–10. Images of crystals of increasing thickness are shown horizontally and images at various microscope defoci are shown vertically.

The absence of interference between diffuse scattering from adjacent defects in the image calculation procedure has been checked for each crystal thickness by comparing the image contrast of $(1\bar{1}00)$ lattice planes adjacent to the twin plane in the TH structure and in the standard

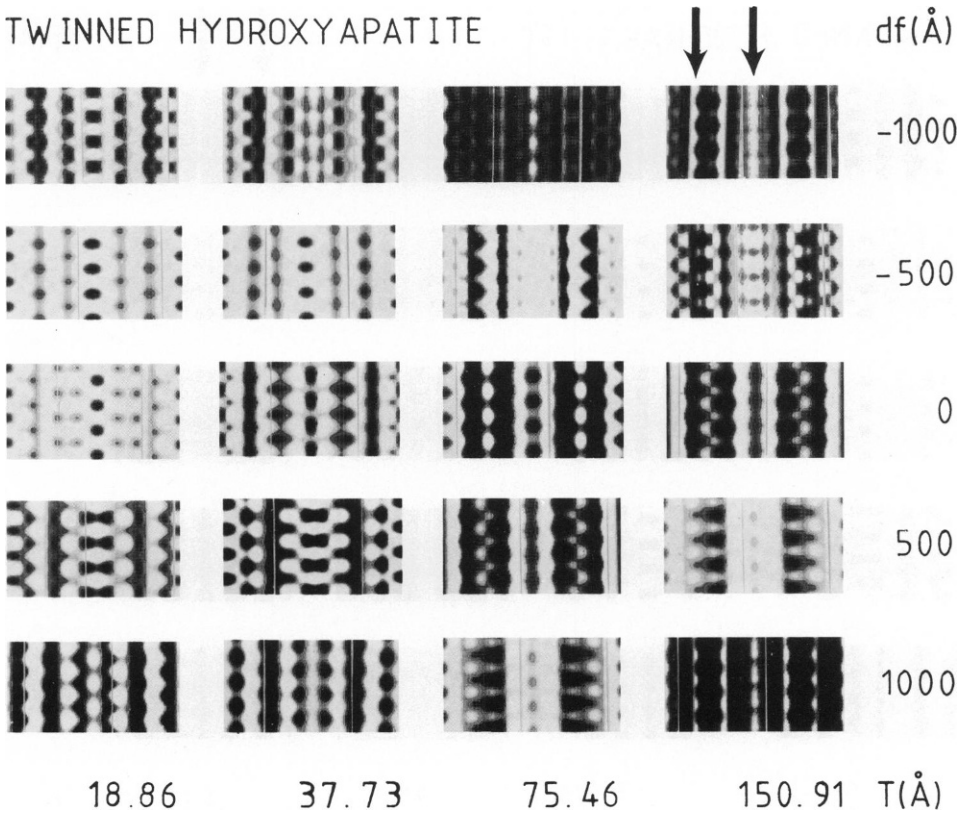

FIGURE 7 Images calculated for the TH structure.

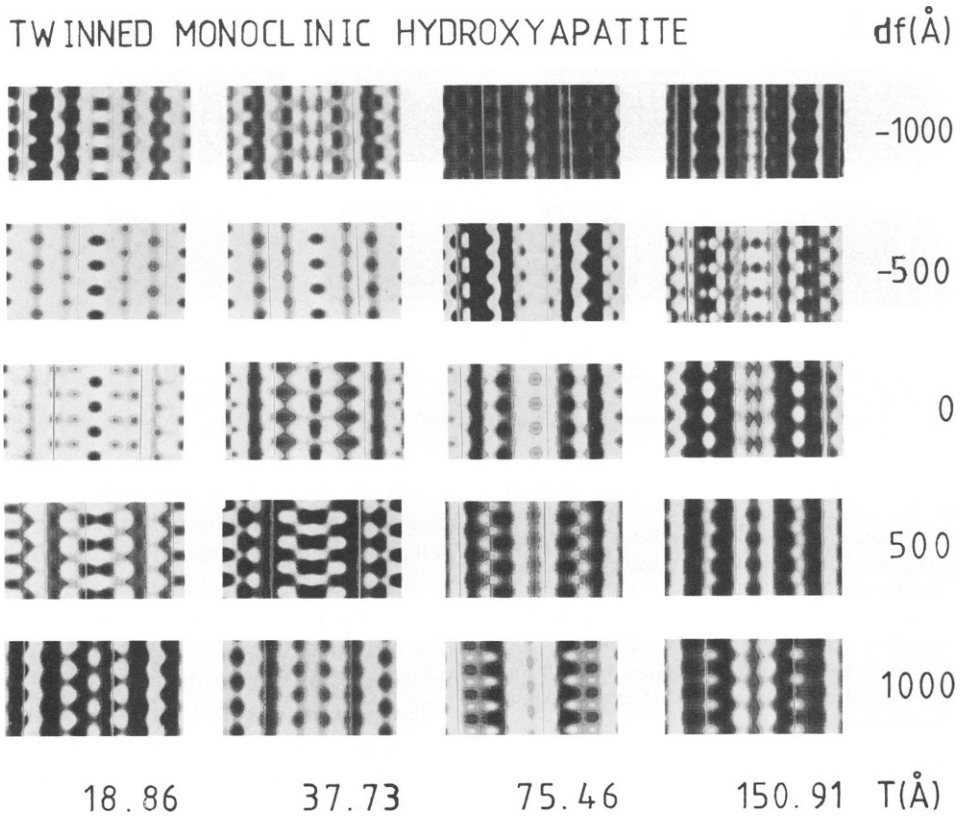

FIGURE 8 Images calculated for the TMH structure.

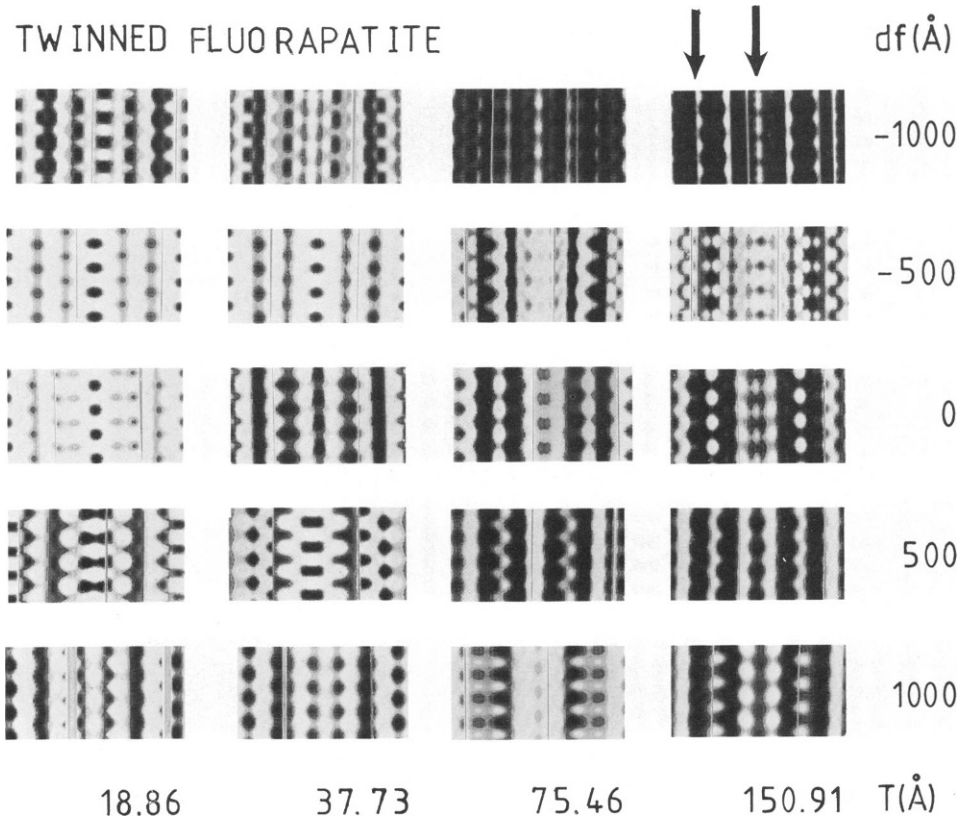

FIGURE 9 Images calculated for the TF structure.

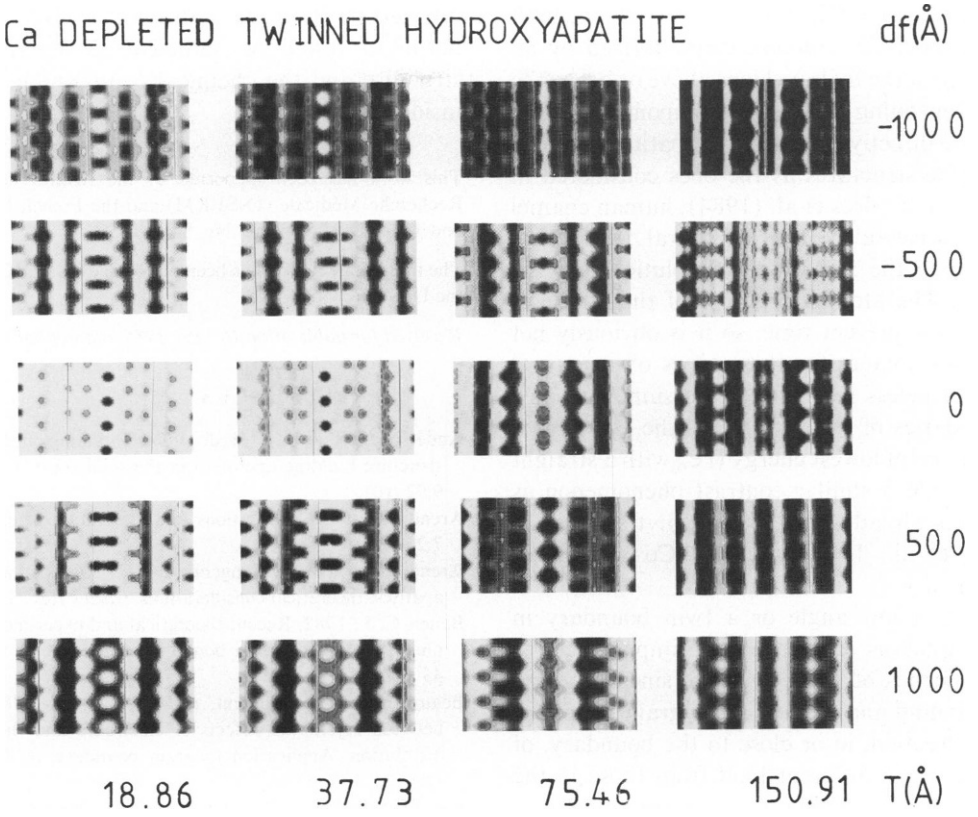

FIGURE 10 Images calculated for the CDTH structure.

hydroxyapatite untwinned structure calculated for the parameters of a high resolution microscope set at Scherzer focus (Fig. 6; see preceding paragraph). On these images the ($1\bar{1}00$) plane and the planes next to it show an identical contrast up to a thickness of 75.46 Å. The ($1\bar{1}00$) lattice plane next to the twin exhibits a contrast which is a compromise between the contrast of an untwinned plane and the contrast of a twin plane. A dramatic contrast difference between ($1\bar{1}00$) planes in the twinned and untwinned structures is observed at a thickness of 150.91 Å.

These observations show the validity of the image calculation for crystal thicknesses up to 75.46 Å. For these crystal thickness values the images calculated can be assumed to correspond to structures with a single defect. This is not the case for images of crystals of thickness above 75.46 Å.

A direct evaluation of each set of calculated images (Figs. 7–10) leads to the following remarks: (*a*) all images corresponding to the same defocus and thickness values are identical in the TH and the TMH structures (Figs. 7 and 8); (*b*) images of the TF and the CDTH structures (Figs. 9 and 10) are different from one another and different from both the TH and TMH images. The DCL appears as a white line in the TH/TMH structures at the following thickness/defocus values: 75.46 Å/−1,000, −500, 500, and 1,000 Å. In the TF structure these values are: 37.73 Å/−1,000 Å; 75.46 Å/−1,000, −500, 0, 500, and 1,000 Å. In the CDTH structure: 37.73 and 75.46 Å/−1,000 Å. The DCL appears as a dark line in the TH/TMH structures at the following thickness/defocus values: 18.86 Å/−500 and 0 Å, and 37.73 Å/−500 Å. In the TF structure these values are: 18.86 Å/−500 and 0 Å; and 37.73 Å/−500 Å. In the CDTH structure these values are: 37.73 and 75.46 Å/−1,000 Å. In all of the other images more specific contrast differences are observed between the defect plane and adjacent ($\bar{1}100$) planes. For example in the TH/TMH structures at a thickness of 18.86 Å and at a defocus of −1,000 Å the contrast at the defect can be characterized by a series of square blobs aligned along this defect while at the adjacent ($1\bar{1}00$) plane these blobs are joined to form a line.

DISCUSSION

In the large majority of the images calculated and for all the structures studied the contrast at the center of the images is different from the contrast at the edges. This strongly shows that the DCL can be created by a diffraction phenomenon arising from a reflection twin parallel to the ($1\bar{1}00$) lattice planes but is little affected by variation of positions of the hydroxyl ions above and below the Ca(2) triangles, as shown by the similarity of the images from the TH and TMH structures. This is in contradiction with Elliott's and Mackie's hypothesis (Elliott and Mackie,

1975) which assumes the DCL is due to a twin plane with components of monoclinic structure characterized by an opposite positioning of the hydroxyl ions above or below the Ca(2) triangles, depending on the twin component.

These results are directly applicable to apatite bicrystals presenting the same structures as the ones considered in this paper. As shown by Brès et al. (1984), human enamel crystals can possess several types of structural defects that can all be related to the anisotropic dissolution and the DCL phenomena. The atomic structure of these defects are not known at the present time, so it is obviously not possible to calculate images for these types of structural defects. It is nevertheless reasonable to assume that low angle grain boundaries of the tilt and/or the twist types parallel to $(1\bar{1}00)$ and of lowest energy (i.e., with a straight interface) would yield a similar contrast phenomenon as the DCL, as it has already been shown for the cases of ceramics (Rühle et al., 1984) and WC-Co composites (Ness et al., 1985).

The presence of a low angle or a twin boundary in human apatite crystals is of considerable importance for the chemical properties of these crystals, since the very essence of the twinning and the low angle grain boundary operations is the creation, in or close to the boundary, of polyhedra of atoms of a different kind from those in the parent structure which provide the opportunity for a crystal to accommodate impurities (Anderson and Hyde, 1974). The chemical composition of grain as well as twin boundaries is rarely identical to that of the parent structure, as shown in a great number of studies concerning the nature of grain boundaries in fields such as solid state chemistry or metallurgy (Briant and Messmer, 1982; Hondros, 1975; Guyot and Simon, 1975; Vitek and Wang, 1982; Bauer, 1982; Cahn, 1982; Hall, 1982). So it is reasonable to assume that such phenomena would also occur for human tooth or bone apatite crystals in the case of the adsorption processes of ions of prime biological interest such as CO_3^{2-}, Mg^{2+}, Pb^{2+}, Sr^{2+}, etc. Furthermore, the microstructural features arising from the strain field generated by a twin or a low angle boundary appear to influence markedly the dissolution reactions in which localized or preferential dissolution occur, such as the type encountered in the carious dissolution process (Voegel and Frank, 1977). Every stage of the dissolution of the bicrystals (the initiation and the propagation stages) are structure-dependent and are therefore strongly affected by the presence of a boundary inside the crystal (Beaumier, 1982; Beaumier et al., 1981).

To develop our understanding of the adsorption and dissolution properties of human apatite crystals it is important to make further progress in the knowledge of the following phenomena: (*a*) the nature of the sites of segregation inside the boundary structure, (*b*) the kinetics of the segregation, and (*c*) the competitive or cooperative multiple segregation phenomena. It is hoped that the use of the most modern medium voltage high resolution electron microscope equipped with microanalysis attachments will permit a resolution sufficient to determine the atomic structure and the chemical composition of the boundary inside the crystals.

This work has been supported by the Institut de la Santé et de la Recherche Médicale (INSERM) and the French Ministry of Research and Technology (contract No. 84-C-1058).

The image calculation has been performed on the ICL 2988 computer at the University of Oxford.

Received for publication 16 May 1985 and in final form 29 May 1986.

REFERENCES

Anderson, S., and B. G. Hyde. 1974. Twinning on the unit cell level as a structure building operation in the solid state. *J. Solid State Chem.* 9:92–101.

Arends, J. 1973. Dislocations and dissolution of enamel. *Caries Res.* 7:261–268.

Arends, J., and W. L. Jongebloed. 1977. Dislocations and dissolution in apatites: theoretical considerations. *Caries Res.* 11:186–188.

Bauer, C. L. 1982. Recent theoretical and experimental advances in the understanding of grain boundary migration. *Journal de Physique.* 43:187–197.

Beaumier, L., M. Froment, and C. Vignaud. 1981. The interactions between crystalline defects of electrodes and the kinetics of anodic dissolution. Application to grain boundary. *J. Electroanal. Chem.* 119:125–135.

Beaumier, L. 1982. Corrosion of grain boundaries: initiation process and testing. *Journal de Physique.* 43(C6):271–282.

Brès, E. F., J. C. Barry, and J. L. Hutchinson. 1984. A structural basis for the carious dissolution of the apatite crystals of human tooth enamel. *Ultramicroscopy.* 12:367–372.

Briant, C. L., and R. P. Messmer. 1982. The effect of impurity elements on chemical bonding at grain boundaries. *Journal de Physique.* 43(C6):225–269.

Cahn, J. W. 1982. Transitions and phase equilibria among grain boundary structures. *Journal de Physique.* 43:199–213.

Cowley, J. M., and A. F. Moodie. 1957. The scattering of electrons by atoms and crystals. I. A new theoretical approach. *Acta Crystallogr.* 10:609–619.

Elliot, J. C., and P. E. Mackie. 1975. Monoclinic hydroxyapatite. *In* Physico-chimie des Apatites d'intèrêt Biologique. G. Monpel, editor. Editions du Cent. Natl. Rech. Sci., Paris. 69–76.

Frazier, P. D. 1968. Adult human enamel I: an electron microscopic study of crystallite size and morphology. *J. Ultrastruct. Res.* 22:1–11.

Gilman, J. J., W. G. Johnston, and G. W. Sears. 1958. Dislocation etch pit formation in lithium fluoride. *J. Appl. Physics.* 29:747–754.

Guyot, P., and J-P. Simon. 1975. Theoretical aspects of the interaction between grain-boundaries and impurities. *Journal de Physique.* 36:141–149.

Hondros, E. D. 1975. Grain boundary segregation, the current situation and future requirements. *Journal de Physique.* 36:117–135.

Jongebloed, W. L., P. J. van den Berg, and J. Arends. 1974. The dissolution of single crystals of hydroxyapatite in citric and lactic acids. *Calcif. Tiss. Res.* 15:1–9.

Kay, M. I., R. A. Young, and A. S. Posner. 1964. Crystal structure of hydroxyapatite. *Nature* (*Lond.*). 204:1050–1052.

Lovell, L. C. 1958. Dislocation etch pits in apatite. *Acta Metallurgica.* 6:775–777.

Lynch, D. F., A. F. Moodie, and M. A. O'Keefe. 1975. *n*-beam lattice images. V. The use of the charge-density approximation in the interpretation of lattice images. *Acta Crystallogr.* 31(A):300–307.

Marshall, A. F., and K. R. Lawless. 1981. TEM study of the central dark line in enamel crystallites. *J. Dent. Res.* 60:1773–1782.

Nakahara, H. 1982. Electron microscopic studies of the lattice image and the "central dark line" of crysallites in sound and carious human dentin. *Bull. Josai Dent. Univ.* 11:209–215.

Nakahara, H., and M. Kakei. 1983. The central dark line in developing enamel crystallites: an electron microscopic study. *Bull. Josai Dent. Univ.* 12:1–7.

Nakahara, H., and M. Kakei. 1984. Central dark line and carbonic anhydrase: problems relating to crystal nucleation in enamel. *In* Tooth Enamel IV. R. W. Fearnhead and S. Suga, editors. Elsevier/North Holland Biomedical Press, Amsterdam. 42–46.

Ness, J. N., W. N. Stobbs, and T. F. Page. 1985. The determination of the mean inner potential of grain boundary films in WC-Co composites by Fresnel techniques. *Proc. EMAG.* 85:523–526.

Nylen, M. U., E. D. Eanes, and K. A. Omnell. 1963. Crystal growth in rat enamel. *J. Cell Biol.* 18:109–123.

O'Keefe, M. A. 1973. *n*-beam lattice images. IV. Computed two-dimensional images. *Acta Crystallogr.* 29(A):389–401.

O'Keefe, M. A., and P. R. Buseck. 1979. Computation of high resolution TEM images of minerals. *Trans. Am. Cryst. Assoc.* 15:27–45.

Patel, A. R., C. C. Desai, and M. K. Agarwal. 1966. Cleavage and etching of prism faces of apatite. *Acta Crystallogr.* 20:796–798.

Phakey, P. P., and J. R. Leonard. 1970. Dislocations and fault surfaces in natural apatite. *J. Appl. Crystallogr.* 3:38–44.

Rachinger, W. A., P. P. Phakey, J. Palamara, and H. J. Orams. 1982. Planar faults in dental hydroxyapatite. *Calcif. Tissue Int.* 34:209–210.

Rönnholm, E. 1962. The amelogenesis of human teeth as revealed by electron microscopy. II. The development of the enamel crystallites. *J. Ultrastruct. Res.* 6:249–303.

Rühle, M., E. Bischoff, and O. David. 1984. Structure of grain boundaries in ceramics. *Ultramicroscopy.* 14:37–46.

Vitek, V., and G. J. Wang. 1982. Atomic structure of grain boundaries and intergranular segregation. *Journal de Physique.* 43:147–161.

Voegel, J.-C., and R. M. Frank. 1977. Stages in the dissolution of human enamel crystals in dental caries. *Calcif. Tissue Res.* 24:19–27.

Voegel, J.-C. 1978. Le cristal d'apatite des tissus osseux et dentaires et sa destruction pathologique. Ph.D. Thesis. Université Louis Pasteur, Strasbourg I, France.

Wood, G. J., W. M. Stobbs, and D. J. Smith. 1984. Methods for the measurement of rigid-body displacements at edge-on boundaries using high resolution electron microscopy. *Phil. Mag. A.* 50:375–391.